



OPEN

The influence of Arctic Fe and Atlantic fixed N on summertime primary production in Fram Strait, North Greenland Sea

Stephan Krisch¹, Thomas J. Browning¹, Martin Graeve², Kai-Uwe Ludwigowski², Pablo Lodeiro¹, Mark J. Hopwood¹, Stéphane Roig¹, Jaw-Chuen Yong^{1,3}, Torsten Kanzow² & Eric P. Achterberg¹✉

Climate change has led to a ~40% reduction in summer Arctic sea-ice cover extent since the 1970s. Resultant increases in light availability may enhance phytoplankton production. Direct evidence for factors currently constraining summertime phytoplankton growth in the Arctic region is however lacking. GEOTRACES cruise GN05 conducted a Fram Strait transect from Svalbard to the NE Greenland Shelf in summer 2016, sampling for bioessential trace metals (Fe, Co, Zn, Mn) and macronutrients (N, Si, P) at ~79°N. Five bioassay experiments were conducted to establish phytoplankton responses to additions of Fe, N, Fe + N and volcanic dust. Ambient nutrient concentrations suggested N and Fe were deficient in surface seawater relative to typical phytoplankton requirements. A west-to-east trend in the relative deficiency of N and Fe was apparent, with N becoming more deficient towards Greenland and Fe more deficient towards Svalbard. This aligned with phytoplankton responses in bioassay experiments, which showed greatest chlorophyll-*a* increases in +N treatment near Greenland and +N + Fe near Svalbard. Collectively these results suggest primary N limitation of phytoplankton growth throughout the study region, with conditions potentially approaching secondary Fe limitation in the eastern Fram Strait. We suggest that the supply of Atlantic-derived N and Arctic-derived Fe exerts a strong control on summertime nutrient stoichiometry and resultant limitation patterns across the Fram Strait region.

The contribution of the Arctic Ocean to global primary production is ~1%^{1,2} but has increased by ~30% between 1998–2012 as a result of surface ocean warming and an associated increase in ice-free ocean surface area³. Iron (Fe) and fixed nitrogen (N) are essential nutrients for phytoplankton, co-regulating growth alongside light availability throughout much of the global ocean^{4–8}. Whilst parts of the high latitude North Atlantic (>50°N) feature Fe limited phytoplankton growth in spring-summer^{9,10}, summertime Arctic primary production is widely thought to be limited by fixed N availability^{11–14} due to low fixed N concentrations across the Arctic basin¹⁵. Direct experimental assessments of (micro)nutrients limiting to phytoplankton growth in the Arctic Ocean are however sparse, despite the pronounced impacts of climate change on this region^{16–18}, potentially altering nutrient fluxes and promoting Fe limitation in the Arctic Ocean^{11,19}.

The Fram Strait region (76–82°N, 20°W–15°E) forms the northern boundary of the Greenland Sea and is the major gateway for water exchange between the Arctic and North Atlantic Oceans (Fig. 1)^{20–22}. The region features two surface currents: (i) the West Spitsbergen Current (WSC) with warm and saline Atlantic Water (4 °C, $S > 35.10$) at its core and a less saline surface layer (<65 m) (Fig. 2a), flowing northwards from the Greenland Sea

¹Marine Biogeochemistry Division, GEOMAR Helmholtz Centre for Ocean Research, 24148 Kiel, Germany. ²Alfred-Wegener-Institute for Polar and Marine Research, 27570 Bremerhaven, Germany. ³Faculty of Science and Marine Environment, Universiti Malaysia Terengganu, 21030 Kuala Nerus, Terengganu, Malaysia. ✉email: eachterberg@geomar.de

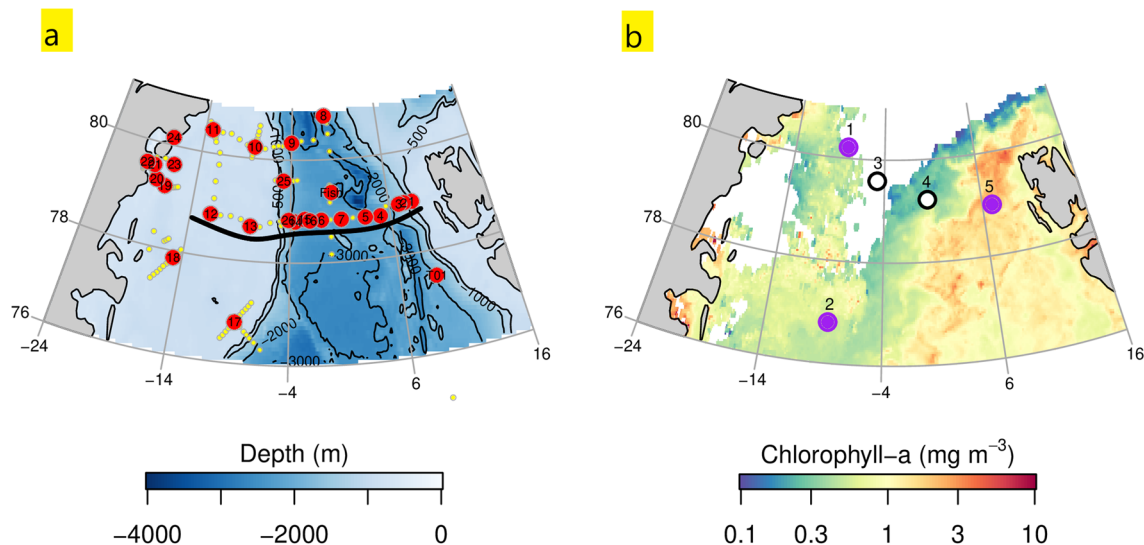


Figure 1. (a) Bathymetry and location of ucCTD stations sampled in the Fram Strait and on the NE Greenland Shelf. Black line highlights the section from which depth profiles are obtained (Fig. 3). (b) Surface chlorophyll-a concentrations (August 2016 average) obtained from MODIS-Aqua (NASA GES DISC)¹⁰⁵. Dots indicate location and outcome of nutrient addition bioassay experiments (E1–E5): Purple = N limitation; white = no response to N, Fe or dust addition. White area indicates sea-ice cover. Figure generated using Matlab software version 9.6.0. (R2019a, Natick, Massachusetts: The MathWorks Inc., 2019).

towards the Arctic Ocean^{22,23}; and (ii) the southward flowing East Greenland Current (EGC), which originates in the Arctic Ocean, includes a contribution of NE Greenland Shelf waters, and constitutes low-salinity Polar Surface Water ($S < 31.40$) and more-saline sub-surface waters ($S < 34.80$) below 50–250 m^{23–25}. About half of the Fram Strait region is covered by seasonal sea ice, leading to strong year-round light limitation of phytoplankton growth^{24,26,27}. However, the extent of Arctic sea ice has diminished considerably over the past three decades (~40%, 1979–2018) (data from the Norwegian Polar Institute, 2020) prolonging the areal extent and duration of enhanced light availability for phytoplankton growth. At the same time, Fram Strait has experienced surface freshening that has driven enhanced water column stratification^{28,29}, potentially linked to variations in the advection and recirculation of Atlantic-derived waters^{16,30,31}. It remains unclear how these on-going physical changes are affecting nutrient supply to surface waters and thereby primary production in the region.

The aim of this study was to assess the factors that currently regulate summertime phytoplankton growth in the Fram Strait region and are hence key to predicting responses of this system to future climate change. We therefore (i) performed a detailed investigation into nutrient and micronutrient concentration distributions and stoichiometry across Fram Strait as part of the GEOTRACES GN05 cruise, and (ii) conducted nutrient addition bioassay experiments as direct assessments of spatial patterns in limiting (micro-)nutrients.

Methods

General. Samples were collected on the RV Polarstern (PS100) as part of the GEOTRACES programme (section GN05). The cruise investigated Fram Strait (> 500 m bottom depth) and the adjacent NE Greenland Shelf (< 500 m, together the ‘Fram Strait region’) in the period 23rd July to 1st September 2016 (boreal summer), which corresponded to the peak melt season. In total, 207 stations were occupied. The water column was sampled with a stainless steel CTD-rosette frame (equipped with SEA-BIRD SBE 911plus) and a powder-coated aluminium GEOTRACES CTD-rosette frame (Seabird, equipped with SBE 911, hereafter ‘ucCTD’). All stations were sampled for macronutrients silicic acid ($\text{Si}(\text{OH})_4$, hereafter Si), phosphate (PO_4), ammonium (NH_4), nitrite (NO_2), and nitrate (NO_3) from the stainless steel CTD. Here we refer to the sum of NH_4 , NO_2 and NO_3 as fixed N. Trace metal micronutrients manganese (Mn), Fe, cobalt (Co), nickel (Ni), copper (Cu) and zinc (Zn) were sampled from the ucCTD at 26 stations (Fig. 1a). Near-surface temperature and salinity were recorded continuously during the cruise from the ship’s thermosalinograph (11 m intake depth). The stainless steel CTD was additionally equipped with a fluorometer (WET Labs ECO AFL/FL).

Nutrient and trace metal analyses. Unfiltered macronutrient samples (NO_2 , NO_3 , PO_4 , Si, NH_4) from the upper 200 m were analysed on board using a QuAatro autoanalyser as per Grasshoff et al.³², modified according to the methods provided by the manufacturer (Seal, Alliance). At all other depths filtered samples (0.2 μm) were frozen and run at AWI following an identical procedure. Measurements were validated against the certified reference material NMIJ CRM 7602a provided by the National Metrology Institute of Japan (see data publication).

Trace metal samples were collected in 24 × 12 L GoFlo bottles (Ocean Test Equipment, OTE) following GEOTRACES sampling and sample handling protocols³³. Briefly, GoFlo bottles were transferred into an over-pressurized clean room (class 100) where water samples were filtered (Acropak 0.8/0.2 μm pore size) into

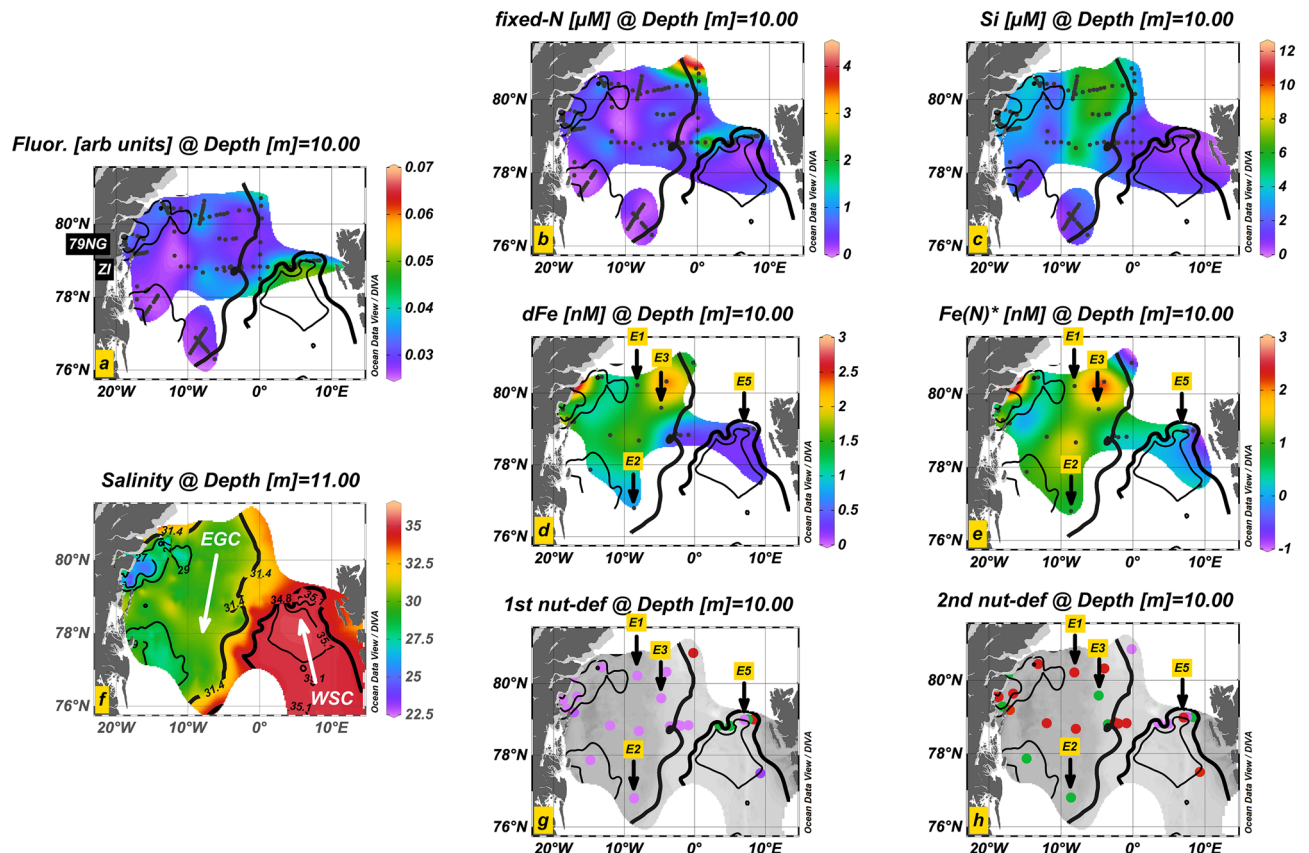


Figure 2. Salinity and nutrient distributions at 10–11 m depths in the Fram Strait region. (a) Salinity, (b) fixed N, (c) Si, (d) dFe, (e) Fe(N)* nutrient deficiency, and (f) fluorescence. Primary (g) and secondary (h) nutrient deficiency after Moore³⁵. Fixed N (purple), dFe (red) and Si (green). Black dots indicate the sampling locations (all 10 m depth). Black arrows indicate sites of bioassay experiments (excl. E4). The location of Nioghalvfjærdsbrae (79NG) and Zachariae Isstrøm (ZI) are depicted in 'a'. Isohalines (contours, 11 m) distinguish the Polar Surface Water ($S < 31.4$, bold) of the southward-directed East Greenland Current (EGC, $S < 34.8$, $< 0^\circ\text{E}$) from Intermediate Water (34.8–35.1) and Atlantic Water ($S > 35.1$, thin black) of the northward-flowing West Spitsbergen Current (WSC). Figure made using Ocean Data View software based on DIVA gridding calculations (Schlitzer, R., Ocean Data View, version 5.2.1, <https://odv.awi.de>, 2020).

pre-cleaned 125 mL low density polyethylene (LDPE) bottles with slight overpressure provided by filtered nitrogen gas (99.999%, AlphaGaz). One additional surface (~2 m) seawater sample was collected in mid Fram Strait using a tow-fish sampling system with suction provided by a Teflon diaphragm pump (Almatec A15). Samples were acidified to pH 1.9 with 180 μL HCl (UpA, ROMIL) and shipped to GEOMAR to determine dissolved concentrations of Mn (dMn), Fe (dFe), Co (dCo), Ni (dNi), Cu (dCu) and Zn (dZn). Trace metal samples were measured via high-resolution inductively coupled plasma-mass spectrometry (HR-ICP-MS) after pre-concentration following the method of Rapp et al.³⁴. Briefly, 15 mL sample aliquots were pre-concentrated using an automated SeaFAST system (SC-4 DX SeaFAST pico; ESI). All reagents for SeaFAST were prepared in de-ionised water ($> 18.2 \text{ M}\Omega \text{ cm}^{-1}$; Milli-Q, Millipore). Single-distilled sub-boiled HNO_3 (SpA grade, Romil) was used for sample elution. Ammonium acetate buffer (pH 8.5) was prepared from glacial acetic acid and ammonium hydroxide (Optima, Fisher Scientific). The tenfold pre-concentrated samples were analysed by HR-ICP-MS (Thermo Fisher Element XR) with quantification via isotope dilution for dFe, dNi, dCu and dZn (^{57}Fe -, ^{62}Ni -, ^{65}Cu - and ^{68}Zn -spike), and standard addition for dMn and dCo (every 10th sample). Measurements were checked against SAFe S reference material (Bruland Research Lab, University of California Santa Cruz) (see data publication).

The deficiency of each nutrient element relative to N was calculated using assumed average phytoplankton stoichiometry ($\text{C}_{7.75}\text{N}_1\text{Si}_1\text{P}_{0.0625}\text{Fe}_{0.469}\text{Mn}_{0.175}\text{Ni}_{0.0625}\text{Zn}_{0.05}\text{Cu}_{0.024}\text{Co}_{0.012}$ (extended Redfield ratio; Ref.³⁵), measured dissolved nutrient concentrations, and the following equation:

$$X_N^* = X_{\text{dis}} - R_{X:N} \bullet N \quad (1)$$

where X_{dis} is the concentration of dissolved nutrient X, N is the concentration of fixed N, and $R_{X:N}$ is the assumed phytoplankton requirement for nutrient X relative to N^{4,35}. Positive values of X_N^* suggest nutrient X is in excess relative to fixed N, while negative X_N^* values indicate nutrient X is deficient relative to fixed N³⁵. Following Moore³⁵ we then ranked the deficiencies for each nutrient at each site using:

$$X'_N = \frac{X_{\text{dis}}}{N \bullet R_{X:N}} \quad (2)$$

The nutrient with minimum X'_N is the most deficient.

Incubation experiments. Incubation experiments were conducted using seawater collected from the OTE Go Flo bottles (~10 m depth; Experiments E1, E2, E3 and E5) or the tow-fish (2 m depth; E4) following procedures described in Browning et al.³⁶. All sampling and sample handling was carried out on-board using trace metal clean techniques under a laminar flow hood. Eighteen trace metal clean, 1 L polycarbonate bottles (Nalgene) were filled with unfiltered seawater. Three bottles were subsampled immediately for assessment of initial conditions. Of the remaining fifteen bottles, three were spiked with fixed N (1 μM nitrate + 1 μM ammonium), three with Fe (2 nM FeCl_3), three with fixed N + Fe, and three with ~10 mg volcanic dust from the Eyjafjallajökull volcanic eruption in 2010 (same sample as described in Achterberg et al.³⁷). The fixed N spike solutions were previously passed through a column of Chelex-100 to remove contaminating trace metals. Three bottles were sealed immediately with no amendment (controls). The lids were sealed with Parafilm and the bottles double-bagged before being placed in an on-deck incubator, which was filled and continuously replenished with near-surface seawater from the ship's underway supply. The incubator was shaded with blue screening (Lee Filters 'Blue Lagoon') to yield incubator light intensities of ~35% of surface values. Samples were incubated for 72 h. Both initial ($t=0$ h) and incubated ($t=72$ h) samples were subsampled for chlorophyll-*a* via filtration of 100 mL sample onto a glass fibre filter (GFF, 0.7 μm nominal pore size, 25 mm diameter, Macherey-Nagel), extracted in the dark in 10 mL 90% acetone at -20 °C (~12 h), then measured using a calibrated Turner Designs Trilogy fluorometer³⁸.

At experimental start sites, samples were collected for determination of macronutrient and trace metal concentrations and phytoplankton pigment concentrations. Samples for phytoplankton pigments were collected by filtration of 2–4 L of seawater onto GFF filters and stored at -80 °C. Upon return to the home laboratory, samples were analysed following van Heukelem and Thomas³⁹. Pigments were extracted in 90% acetone in plastic vials using glass beads in a cell mill, centrifuged (10 min, 5,200 rpm, 4 °C), and then the supernatant was filtered through PTFE filters (0.2 μm pore size, VWR International) and analysed by reverse-phase HPLC (Dionex UltiMate 3,000 LC system, Thermo Scientific). Pigment standards were acquired from Sigma-Aldrich (USA) and the International Agency for ¹⁴C Determination (Denmark). Pigment compositions were converted to the approximate contribution of different phytoplankton types to total chlorophyll-*a* using CHEMTAX⁴⁰ with starting pigment ratios from Coupel et al.⁴¹.

Results and discussion

Nutrient distributions. Fixed N displayed an east to west gradient in surface waters (10 m depth) (Fig. 2b). Maximum surface concentrations were found in the WSC (0.7 ± 1.0 μM , mean value \pm standard deviation) and at the northern-most stations in Fram Strait (1.4 ± 1.1 μM , 80.2 – $80.8^\circ\text{N}/0$ – 4°W). Elsewhere, relatively low fixed N concentrations were observed (0.3 ± 0.3 μM). Surface Si showed a north-to-south gradient within the eastern part of the EGC (Fig. 2c). Highest Si concentrations were found at higher latitudes (4.2 ± 1.6 μM at all EGC stations $>79^\circ\text{N}$), whereas lower Si concentrations were found at the NE Greenland Shelf break to the south (1.2 ± 0.5 μM at all EGC stations $<77^\circ\text{N}$). The WSC was depleted in Si (0.7 ± 0.7 μM), which contrasted to the EGC with elevated Si (3.5 ± 2.9 μM for all stations in the EGC). Surface dFe displayed maxima on the shelf at glaciated stations close to the Greenlandic coast (Fig. 2d; S19–S24, 1.8 ± 1.0 nM). DFe concentrations within the EGC (1.3 ± 0.6 nM) exceeded those in the WSC (0.4 ± 0.1 nM) by a factor of 3–4. In Fram Strait, dFe showed a similar trend to Si and was elevated at the two northern-most stations in its central and western parts (S8, 1.3 nM; S9, 2.5 nM), in contrast to the observed minimum dFe in the central WSC in the eastern Fram Strait (S4, 0.2 nM). Collectively, dFe and Si both showed elevated concentrations at low salinity (Fig. S1), which was most evident at the eastern boundary of the Polar Surface Water (0 – 10°W). In contrast to dFe and Si, no clear special pattern in surface fixed N concentrations relative to salinity was observed across the study region.

Concentrations of N and Si uniformly increased with depth, whereas depth profiles of dFe showed much greater spatial variability (Fig. 3c–e). Water column distributions of fixed N, Si and dFe in the WSC were distinctly different from the EGC. In the WSC, fixed N and Si were depleted (<5 μM) above ~25 m and ~450 m, respectively. In the EGC, fixed N remained depleted to greater depths nearer Greenland (21–148 m), and mean concentrations were lower (6.1 $\mu\text{M} \pm 4.3$ μM for salinities <34.8 , corresponding to depths <20 – 454 m) compared to the WSC (9.4 $\mu\text{M} \pm 3.7$ μM in the water column at salinities >35.1 , corresponding to depths <71 – 261 m). Si on the contrary was enriched in the EGC (5.4 $\mu\text{M} \pm 2.3$ μM) relative to the WSC (3.7 $\mu\text{M} \pm 1.3$ μM). The distribution of Si at depth followed the spatial pattern found in surface concentrations, showing a north-to-south gradient in the water column of the EGC. Elevated concentrations were observed at higher latitudes (all EGC stations $>79^\circ\text{N}$), near the glacial termini of Zachariæ Isstrøm and Nioghalvfjærdsbrae (6.3 $\mu\text{M} \pm 3.2$ μM) and at the NE Greenland Shelf break (5.8 $\mu\text{M} \pm 1.3$ μM , EGC stations 4 – 8°W) compared to lower latitudes (3.8 ± 1.8 μM , EGC stations $<77^\circ\text{N}$). Enhanced Si concentrations (>10 μM) on the inner-Greenlandic shelf at depth likely reflect elevated benthic inputs⁴². Mean EGC dFe concentrations (1.1 nM ± 0.5 nM) were ~twofold elevated over WSC values (0.5 nM ± 0.2 nM). Depth profiles of dFe showed sporadic enrichment (>1 nM) that coincided with dMn (Fig. 3f) at multiple depths near Svalbard's continental slope, likely derived from sedimentary inputs as has been observed elsewhere in the high latitude North Atlantic^{43,44}, and in central Fram Strait. Enrichment of dFe in the EGC was more sporadic than for Si, likely as a consequence of rapid scavenging of dFe sources along the Greenlandic shelf^{45,46}. However, as for Si, dFe displayed maxima in the water column off Zachariæ Isstrøm and

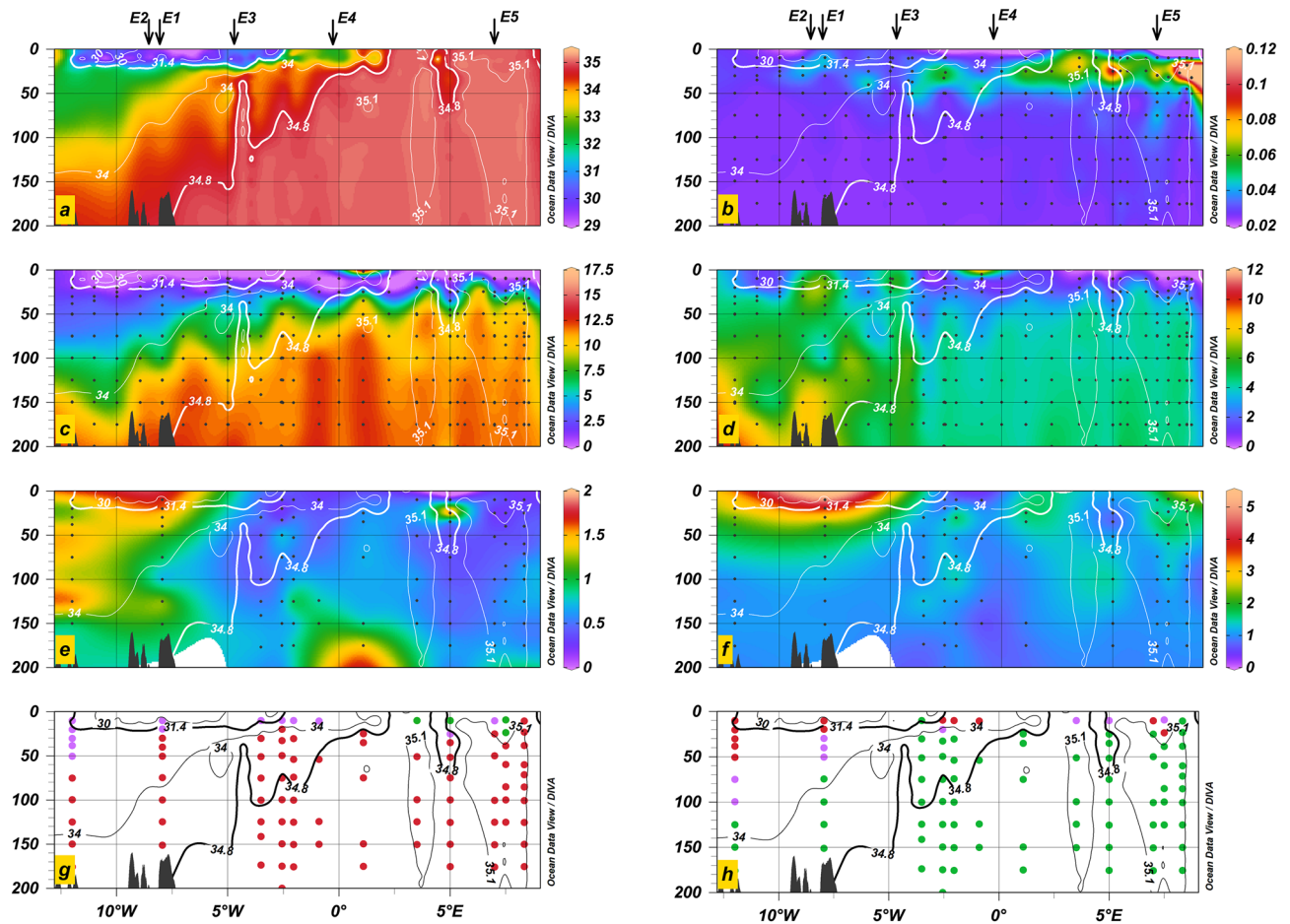


Figure 3. Fram Strait sections (79°N) of (a) salinity, (b) fluorescence (arb. units), (c) fixed N (μM), (d) Si (μM), (e) dFe (nM) and (f) dissolved manganese (nM), (g,h) derived primary and secondary nutrient deficiency (see Eq. (2)). Fixed N (purple), dFe (red), Si (green) and dCo (orange). Black arrows (top panel) indicate the longitudinal positions of the nutrient addition bioassay experiments. The location of the presented section is shown in Fig. 1a. Isohalines (contours) indicate the presence of Polar Surface Waters ($S < 31.4$, bold) as part of the East Greenland Current ($S = 34.8$, bold), Intermediate Water ($34.8 < S < 35.1$) and core Atlantic Water ($S > 35.1$). Black dots in b–f indicate the sample depths. Figure made using Ocean Data View software based on DIVA gridding calculations (Schlitzer, R., Ocean Data View, version 5.2.1, <https://odv.awi.de>, 2020) and RTopo-2.0.1 bedrock topography¹⁰⁶.

Nioghalfjærdsbrae (S20, S22, S24, $1.5 \text{ nM} \pm 0.6 \text{ nM}$) and near the NE Greenland shelf break (S9, S10, S12, S13, $1.2 \text{ nM} \pm 0.5 \text{ nM}$) indicating similar shelf-associated Si and dFe sources.

A similarly extensive survey of macronutrient distributions in the Fram Strait region was previously conducted in July–August 2008. Our observations of fixed N (Jul–Aug 2016) agree well with these previous measurements, showing surface depletion ($< 5 \mu\text{M}$) increasing in depth from the WSC (16–42 m) to the EGC (12–129 m)^{47,48}. Mean fixed N concentrations within the EGC ($6.1 \pm 4.3 \mu\text{M}$ in all EGC stations $S > 34.8$) were comparable to observations made in 2008 ($5.3 \pm 4.1 \mu\text{M}$), but fixed N was somewhat higher in the WSC ($9.4 \pm 3.7 \mu\text{M}$ in the water column at salinities > 35.1) compared to 2008 ($5.7 \pm 4.2 \mu\text{M}$), possibly related to increased advection and/or recirculation of Atlantic Water to the Fram Strait region in 2016^{30,31}. Surface fixed N in the WSC ($0.7 \pm 1.0 \mu\text{M}$) was similar to 2008 ($0.9 \pm 1.2 \mu\text{M}$), and falls between observations of the upstream Irminger Basin ($2.3 \pm 1.7 \mu\text{M}$, Jul–Aug 2010) and the downstream Arctic Ocean (Aug 2014) where complete depletion of surface Atlantic Water fixed N ($< 0.02 \mu\text{M}$) is evident^{49,50}. Atlantic Water is thus an essential source of fixed N to the Fram Strait region⁵¹. The distribution of Si showed an east-to-west gradient in 2008 similar to 2016, with elevated concentrations in the EGC at high latitudes ($5.2 \pm 2.2 \mu\text{M}$, in all EGC stations $> 79^\circ\text{N}$) relative to lower latitudes ($4.6 \pm 2.2 \mu\text{M}$ in all EGC stations at 77°N). This north–south gradient was most pronounced for surface Si ($2.6 \pm 1.2 \mu\text{M}$, $> 79^\circ\text{N}$; $1.4 \pm 0.2 \mu\text{M}$ at 77°N), and is further evident when considering Si concentrations further north from within the Transpolar Drift ($12.9 \pm 0.6 \mu\text{M}$, Sep 2015)^{52,53}, and further south from the EGC bordering the Irminger Basin ($1.4 \pm 0.7 \mu\text{M}$ at 20 m, $58.1\text{--}60.0^\circ\text{N}/35.0\text{--}42.7^\circ\text{E}$, Jul–Aug 2010)⁵⁰. DFe shows the same north–south trend, with concentrations $>$ twofold elevated in the surface Transpolar Drift ($2.9 \pm 1.3 \text{ nM}$)^{53,54}, and an order of magnitude further depleted in the Iceland ($0.1 \pm 0.1 \text{ nM}$) and Irminger Basins ($0.1 \pm 0.2 \text{ nM}$)^{9,50}. EGC dFe and Si may thus

		E1	E2	E3	E4	E5
Lat	°N	80.22	76.80	79.59	79.36	78.99
Long	°E	-8.14	-8.61	-4.77	0.23	6.99
T _{pot}	°C	-1.3	0.1	-1.6	2.7 [‡]	8.8
Sal	PSU	29.97	30.62	30.03	32.67 [‡]	35.07
MLD [§]	m	12	10	14	/	14
NO ₃	μM	<0.02	<0.02	0.5	12.3	0.3
PO ₄		0.4	0.3	0.3	1.0	0.1
Si		4.4	1.1	4.4	7.4	<0.03
NH ₄		<0.05	<0.05	0.5	1.6	<0.05
dCo	pM	202	148	164	114*	40
dFe	nM	1.3	0.8	1.8	1.3*	0.4
dMn		5.0	4.2	5.6	2.8*	1.5
dNi		6.2	4.7	5.9	4.4*	3.1
dCu		4.8	3.7	4.5	2.9*	1.3
dZn		1.8	/	1.8	0.9*	0.8
Fe _N * initial	nM	1.3	0.8	1.3	-5.3*	0.3
Initial	Chl.a in mg/m ³	0.82	0.25	0.16	0.15	0.51
Control		0.69	0.13	0.18	0.09	0.49
+N		2.16	0.82	0.15	0.09	1.18
+Fe		0.54	0.25	0.16	0.09	0.51
+N + Fe		1.47	0.45	0.15	0.09	1.30
+Dust		0.73	0.23	0.16	0.08	0.59
N-to-initial		%	313	628	80	58
(N + Fe)-to-initial	213		344	80	96	265

Table 1. Initial conditions of bioassay experiments, and chlorophyll-a biomass response to nutrient amendments. [§]Surface mixed layer depth (MLD) defined by threshold value of 0.03 kg/m³ difference to surface reference density (10 m depth). [‡]Values obtained from ship-based thermosalinograph (11 m depth). *Trace metal concentrations taken from station S8.

share a common regional source in the Arctic Ocean, and may themselves in turn be a source to the Greenland Sea phytoplankton communities.

Phytoplankton abundance and community structure. Satellite-derived surface chlorophyll-a concentrations showed an east-to-west transition in phytoplankton standing stocks in August 2016, with minima in Central and Western Fram Strait, and maxima in Atlantic Waters northwest of Svalbard (Fig. 1b). Laboratory-determined chlorophyll-a concentrations matched the satellite-derived trend for the WSC (0.5 μg L⁻¹), Western and Central Fram Strait (0.2 μg L⁻¹), yet indicated highest phytoplankton concentrations in the EGC on the outer NE Greenland Shelf (0.8 μg L⁻¹) (Table 1). Measured pigment assemblages and associated CHEMTAX data analysis suggested an east to west transition in surface phytoplankton community composition that correlated with the region's nutrient and current regimes (Figs. 2 and 4a). On the Si- and dFe-replete NE Greenland shelf, diatoms were the dominant phytoplankton group (E1–E2, 80% of chlorophyll-a was attributable to diatoms). A similar dominance has been observed elsewhere in coastal Greenlandic waters which remain Si-replete post-spring bloom^{55,56}. The diatom contribution decreased alongside surface Si and dFe concentrations towards western Fram Strait (E3, 27%) and central Fram Strait (E4, 25%) and was lowest in eastern Fram Strait (E5, 1%). The Eastern Fram Strait phytoplankton composition was dominated by haptophytes (E5, 68%) matching earlier observations in the Si-depleted summer WSC⁵⁷. Haptophyte contribution declined considerably to central Fram Strait (E4, 17%) and was almost absent at western Fram Strait (E3, 2%) and on the NE Greenland Shelf (E1–E2, 0–1%). Whilst both the NE Greenland shelf and eastern Fram Strait showed dominance of either diatoms or haptophytes, stations located in western (E3) and central (E4) Fram Strait exhibited mixed assemblages of phytoplankton including enhanced contributions of cryptophytes (10% and 28% respectively), and prasinophyceae (31% and 9%).

Nutrient limitation. Phytoplankton responses to nutrient amendment were assessed via changes in chlorophyll-a concentrations, which likely reflects contributions from both bulk phytoplankton biomass changes and enhances in chlorophyll-a: carbon ratios following supply of limiting nutrient(s)^{58,59}. Chlorophyll-a concentrations increased significantly relative to untreated controls following addition of fixed N in Experiments 1, 2, and 5 and did not vary following supply of any nutrient combination in Experiments 3 and 4 (Fig. 4b–f). For Experiments 1, 2, and 5, relative chlorophyll-a increases following N supply were larger in experiments around the EGC shelf break (mean increases of +313% in E1; +628% in E2) than in the WSC in eastern Fram Strait (+241% in E5). Our observations of significant chlorophyll-a increases following N supply in these experiments suggested

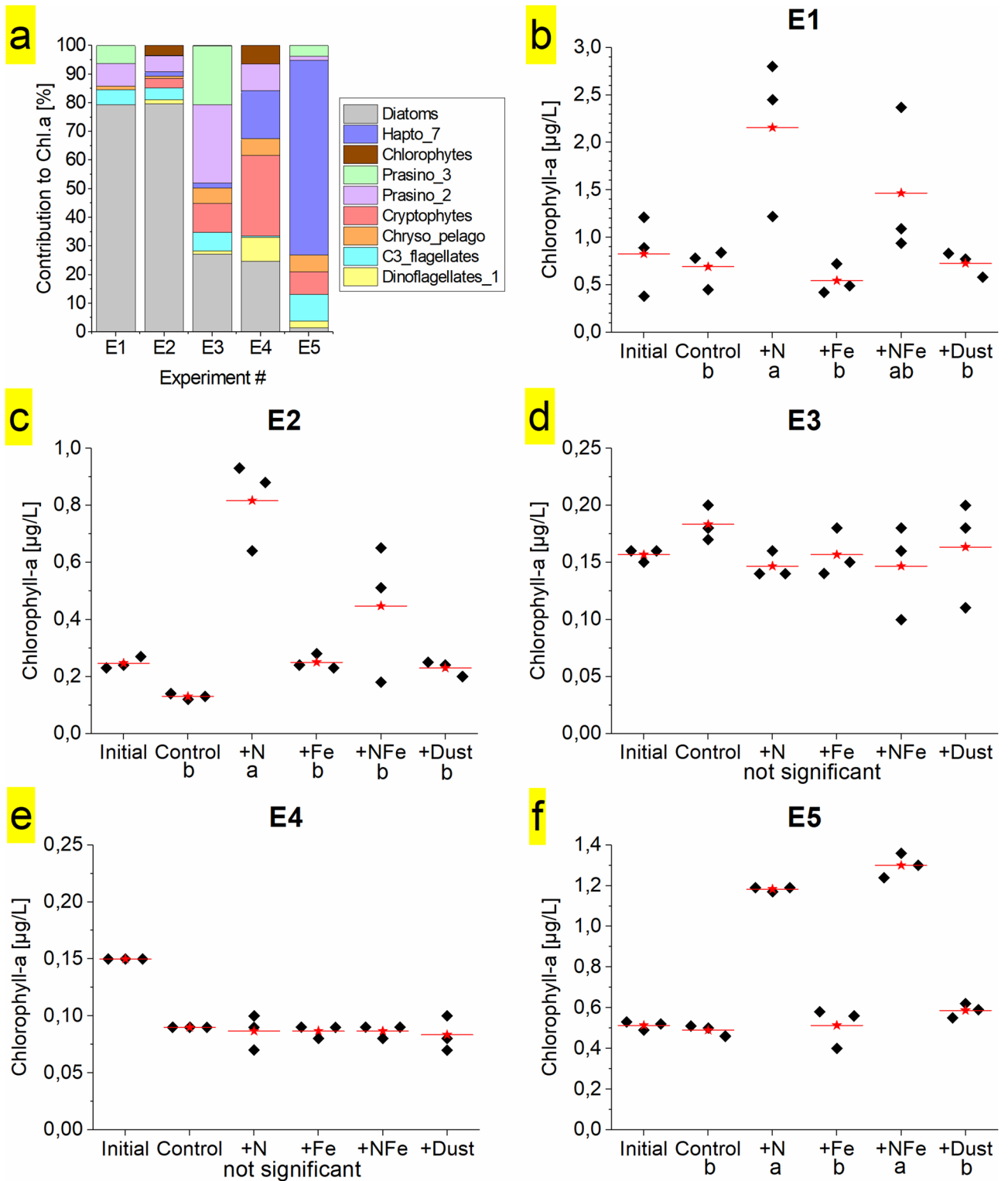


Figure 4. Phytoplankton community composition and responses to nutrient supply at incubation sites. (a) Phytoplankton community composition at bioassay experiment water collection sites as determined by pigment analysis and CHEMTAX. (b–f) Chlorophyll-a responses to nutrient additions. Red symbols show the mean chlorophyll concentration and black symbols indicate the individual replicates. Treatments labelled with the same letter have statistically indistinguishable means (ANOVA followed by a Tukey Honest Significant Difference test, $P \leq 0.05$, $n = 3$). Figure generated using OriginPro software, version 9.1.0 (OriginLab Corporation, Northampton, MA, USA).

that fixed N was the primary summertime limiting nutrient through these parts of the Fram Strait region during our cruise occupation. These observations are consistent with prior work on the NE Greenland Shelf⁶⁰ and elsewhere in the Arctic Ocean^{11,13,61–63}. Although not statistically significant, small additional enhancements in chlorophyll-a concentrations were observed in the Experiment 5 N + Fe treatment over + N alone (+265% in comparison to +241% for N addition alone), suggesting that Fe was potentially a secondary limiting nutrient after N in the surface WSC. The absence of any significant chlorophyll-a enhancements in response to supply of the volcanic ash dust in any of the experiments suggested that the dust was not a significant source of fixed N, as anticipated based on the results of previous bioassays and leaching experiments with this ash sample³⁷.

No statistically significant responses to any of the supplied nutrient combinations relative to unamended controls were found in Experiments 3 and 4, located in the western and central Fram Strait respectively. This could either be a result of (i) limitation by an alternative resource (light or another nutrient); (ii) grazer regulation of the phytoplankton community, maintaining phytoplankton standing stocks despite enhanced specific growth rates following nutrient supply (e.g., Mann and Chisholm⁶⁴); or (iii) restricted net phytoplankton community growth over the experimental duration (72 h) due to low starting biomass concentrations and/or cold temperatures⁶⁵. Our results do not allow us to unambiguously distinguish between these; however, ancillary observations allow identification of the most probable factors. Light limitation of the ambient phytoplankton community at these sites was unlikely, as surface mixed layers were shallow (14 m at Experiment 3, Table 1), irradiances were elevated (E3: up to 395 W m⁻², E4: up to 478 W m⁻²), and day lengths long (19–24 h). Furthermore, in-situ light limitation, if present, would likely be at least partially relieved following incubation on-deck, leading to chlorophyll-a increases in control samples^{66,67}, which were not observed. (Co-)limitation of phytoplankton growth by another element cannot be ruled out, however concentrations of all measured nutrients were elevated, arguing against this (Table 1). In addition, the absence of any response following the volcanic dust addition, which likely supplied a range of trace metal micronutrients alongside Fe³⁷, suggested that non-Fe trace elements were also not primary limiting nutrients. Slow, nutrient-replete growth, low starting phytoplankton concentrations, in combination with top-down grazer regulation therefore appears the most likely cause of the lack of net community growth response in these two experiments.

Nutrient deficiency. The nutrient concentrations in seawater relative to typical phytoplankton requirements provide the capacity to predict which nutrient becomes limiting to phytoplankton growth³⁵. Either fixed N or Fe was calculated to be the most deficient nutrient in surface waters of the Fram Strait region (that is, had lowest concentrations in seawater taking into account assumed-average phytoplankton requirements; Eq. (2), Fig. 2). An east-to-west transition was found in the deficiency of Fe relative to N (Fe_N^*). Surface waters of the EGC, where fixed N limitation was observed, showed positive Fe_N^* (mean 1.1 ± 0.9 nM, range -0.3 to 3.2 nM), which increased towards the Greenlandic coast and the glaciated Zachariæ Isstrøm (S20, 1.7 nM) and Nioghalvfjerdsbrae Glacier (S21, 1.2 nM; S24, 3.3 nM) (Fig. 3d). Interestingly, the station closest to Nioghalvfjerdsbrae exhibited the EGC minimum in Fe_N^* (-0.3 nM, S22), likely a result of low dFe/ low fixed N meltwater discharge in combination with dFe scavenging removal^{14,45}. The surface WSC showed lower Fe_N^* (0.1 ± 0.4 nM, -0.7–0.3 nM), with decreasing values towards the Svalbard shelf break. The station closest to Svalbard (S1) had lowest Fe_N^* (-0.7 nM) at low residual dFe (0.3 nM), suggesting phytoplankton may have been approaching a situation of co-limitation by Fe and N^{10,36,68}. This is in agreement with the results of Experiment 5, where an enhanced chlorophyll-a response to Fe + N amendment over + N alone was apparent. In addition, some surface waters of the WSC also showed Si deficiency relative to fixed N, suggesting that this nutrient might be (co-)limiting for Si-requiring diatoms in this location and potentially, alongside low N and Fe levels, partly explaining their absence in these waters (Figs. 3g and 4). Elsewhere, Si was generally in excess relative to N.

Subsurface (> 10 m) waters were always Fe deficient relative to fixed N throughout the central Fram Strait region (Fig. 3g), presumably caused by remineralisation-driven increases in macronutrient concentrations, which are not reflected in dFe as a result of the high particle reactivity and scavenging removal of this element^{35,69}. Sub-surface N-deficiency was only observed on the NE Greenland Shelf where the nitracline was deeper, suggested to be a consequence of release of low N glacial meltwater, or more generally strong stratification driven by freshwater. Making the assumption of a phytoplankton requirement for Si, this element was typically calculated as the second most deficient nutrient throughout subsurface waters (Fig. 3h). Repeating the analysis with Si excluded instead showed widespread secondary deficiency by dissolved Co.

Factors controlling nutrient limitation in Fram Strait. Like other marine regions, the drivers of phytoplankton nutrient limitation patterns strongly depend on the relative supply: demand ratio for each nutrient⁴. In order to categorize measured nutrient concentrations in terms of limitation potential, we assumed fixed elemental requirements for phytoplankton. The potential for high variability in elemental quotas of phytoplankton, particularly under reduced competition that exists in monoculture, has been reported⁷⁰. However, the success of nutrient deficiency calculations in correctly predicting the identity of the growth limiting nutrient in the ocean (i.e., following direct experimental determination or via molecular nutrient stress signatures) argues for a relatively conserved, community-level elemental stoichiometry in natural phytoplankton communities^{4,36,71}. Changes in nutrient limitation patterns, and in particular the presence of N versus Fe limitation, or the development of co-limitation, will therefore likely have a strong dependence on altered supply rates and ratios of these nutrients to the surface ocean^{36,72}.

In this respect, the southward flowing EGC and the northward flowing WSC are distinctly different in physical characteristics, nutrient content, and thereby nutrient supply to surface waters. The EGC was colder and fresher, with regionally-averaged concentrations having lower fixed N but 2–fourfold higher Si and dFe compared to the WSC (Table 2). Intermediate Waters, defining the boundary between these two water masses, showed values

		EGC	IW	WSC
T_{pot}	°C	-0.5 ± 0.7	-0.4 ± 2.2	8.3 ± 0.7
Sal	PSU	30.37 ± 0.78	32.43 ± 1.97	35.02 ± 0.06
Fixed N	μM	0.3 ± 0.5	0.6 ± 0.6	0.7 ± 1.0
dFe	nM	1.5 ± 0.8	0.8 ± 0.5	0.4 ± 0.1
Si	μM	3.5 ± 2.9	2.3 ± 1.2	0.7 ± 0.7

Table 2. Region-averaged physical characteristics and nutrient concentrations (mean value \pm standard deviation) of the East Greenland Current (EGC), West Spitsbergen Current (WSC), and Intermediate (IW) surface (10 m) waters.

between these end members, which may have been derived from the convergence of the EGC and WSC^{23,25,73}. Elevated dFe and Si in the EGC was likely a result of locally-derived freshwater and southward transport in the Transpolar Drift, itself fuelled by riverine discharge to the Eurasian Arctic Shelf^{45,74,75}. Conversely, these sources supply low amounts of fixed N^{14,52,53}. In addition to the low N:P ratio of Pacific water, which is advected across the Arctic and exits via Fram Strait^{15,76}, this may be a contributing factor to the observed primary N limitation of the phytoplankton community in this region (Figs. 3 and 4). In contrast, North Atlantic source waters supplying the WSC are depleted in Fe and Si, alongside N, which leads to conditions approaching serial N-Fe limitation (and potential co-limitation by Si for diatoms) in the eastern Fram Strait^{10,67,77}. Further north, a branch of the WSC continues to flow into the SE Nansen Basin, where – off-axis to the dFe-rich Transpolar Drift—Fe deficiency (i.e. $\text{Fe}_N^* < 0$) has also been reported^{19,74}.

Prior work has shown that southward transport of N associated with the EGC ($124 \pm 22 \text{ Tg yr}^{-1}$) is almost balanced by northward transport associated with the WSC ($92 \pm 17 \text{ Gg yr}^{-1}$)⁵¹. Surface Waters of the Fram Strait region were N depleted ($0.5 \pm 1.2 \mu\text{M}$), but deeper waters below the mixed layer hosted enhanced fixed N concentrations (15–500 m, $8.4 \pm 4.1 \mu\text{M}$) (Fig. 3). Summer mixed layer depths in Fram Strait are shallow (10–23 m measured on the PS100 cruise, Table 1) and deep-water reservoirs are thus unlikely a substantial source of fixed N to the surface ocean at this time⁴⁹. Conversely, in winter, deep mixing to depths > 100 m below the nutrient-depleted surface layer (10–25 m), replenishes surface waters of Fram Strait region with N^{15,78}. Rates of surface WSC fixed N replenishment may be an order of magnitude greater during autumn/winter than summer^{49,79}, making deep winter mixing likely the dominant factor controlling the extent of annual new primary production in the Fram Strait region⁸⁰. Deep-water re-supply of surface Fe is more restricted, due to deeper ferriclines that are observed to depths > 150 m in the WSC of Fram Strait (Fig. S2). Therefore to account for near-complete drawdown of fixed N between winter and summer in the WSC, Fe must have additional supply routes (assuming that seasonally or regionally enhanced regeneration/recycling of Fe cannot fully account for such drawdown⁸¹). Aside from transient, low-frequency events such as volcanic eruptions³⁷ or agricultural and forest fires⁸², atmospheric deposition of Fe across the Arctic is reportedly low^{83,84}. This suggests a dominance of sediment supplied Fe from shallow bathymetry to the south (i.e. coastal Greenland and Svalbard) and supply of Arctic-derived Fe by the Transpolar Drift to the EGC waters (offshore Fram Strait region)⁷⁵. The importance of sedimentary dFe supply to Fram Strait region was also indicated from the distribution of dissolved Mn (Fig. 3f), which derives primarily from sediments and shows maxima in (i) the surface EGC where the influence of the Transpolar Drift is expected⁸⁵, (ii) near the glacier termini on the NE Greenland Shelf, and (iii) on the continental slopes of Svalbard^{86–88}.

Future perspectives. Our finding of widespread N deficiency in nutrient concentration fields alongside direct experimental evidence for N limitation points towards the importance of variability in N sources in regulating summertime phytoplankton productivity in Fram Strait. Consistent with prior studies, we corroborate that northward advection of Atlantic-derived fixed N is essential to sustain primary production in the N-depleted western Fram Strait and on the NE Greenland Shelf^{4,24,60,79}. Accordingly, we suggest that the future areal and seasonal extent of primary production in Fram Strait region might be strongly impacted by changes in the lateral advection of fixed N via the WSC, in addition to an earlier onset of phytoplankton growth resulting from reduced ice cover^{79,89}. As an Arctic outflow region, Fram Strait is clearly strongly affected by processes occurring within the Arctic. Broad-scale changes to Arctic inflow, sea-ice cover, lateral advection via the Transpolar Drift and wind driven mixing will all have downstream effects on nutrient stoichiometry in Fram Strait^{80,90,91}. How lateral and vertical nutrient supply will change in the future Arctic as a result of on-going changes to sea-ice retreat and stratification remains uncertain, as neither lateral transport of nutrients in the Transpolar Drift, or vertical turbulent supply of nutrients during summer are well quantified^{13,75,92}.

Surface primary production in the Arctic Ocean due to increased summertime light availability has increased during the past few decades^{3,93}. Second to light limitation, Arctic Ocean net primary production seems foremost limited by the availability of fixed N^{15,80} and may at some point hinder future increases in productivity, although changes in nutrient supply ratios and/or phytoplankton species composition may result in other nutrients such as Si, PO_4 or dFe to become limiting factors as well^{11,94}. In the future, the Arctic Ocean is projected to have less ice coverage and become fresher and more stratified, which would reduce winter mixing depth and the associated supply of deep water nutrients^{8,95}. Yet, conversely sea-ice loss also facilitates increased wind driven mixing, which is thought to have enhanced autumn productivity in some Arctic regions^{96,97}, and may also offset nutrient

limitation caused by water column stratification in Fram Strait region. Additionally, some modelling suggests that decreasing sea-ice cover may lead to increased import of Atlantic Waters—and thus, fixed N—to the Fram Strait region⁹⁸. Therefore in addition to changes in the areal extent of ice-free ocean^{27,99,100} any future projection of primary production in the Fram Strait region is also hampered by poor knowledge of changes in nutrient supply as a result of the strong seasonal and inter-annual variability in current regimes^{31,73}, changes in phytoplankton community composition and their nutrient requirements^{57,65,101}. This compounds a poor mechanistic understanding of what drives elevated dFe and Si concentrations in the Transpolar Drift and how this will respond to future climate perturbations^{19,45,75}. In addition, the relative importance of N₂ fixation by diazotrophs in this region is poorly quantified^{102–104}. Diazotrophs have particularly high Fe requirements, therefore the distribution of dFe, which in Fram Strait appears to be predominantly supplied by the EGC, could also be important for controlling their distribution and the rate of new fixed N introduced into this system by this process.

Data availability

All data used throughout this publication is accessible online. PS100 (GN05) physical oceanography data can be obtained from: <https://doi.pangaea.de/10.1594/PANGAEA.871030> (ucCTD), and <https://doi.pangaea.de/10.1594/PANGAEA.871028> (stainless steel CTD), and <https://doi.pangaea.de/10.1594/PANGAEA.873158> (ship-based thermosalinograph). PS100 (GN05) macronutrient data can be obtained from: <https://doi.pangaea.de/10.1594/PANGAEA.905347> (ucCTD), and <https://doi.pangaea.de/10.1594/PANGAEA.879197> (stainless steel CTD). PS100 (GN05) bioassay data, and dissolved trace metal data will be made available on Pangaea database following this publication.

Received: 29 May 2020; Accepted: 25 August 2020

Published online: 17 September 2020

References

- Pabi, S., Van Dijken, G. L. & Arrigo, K. R. Primary production in the Arctic Ocean, 1998–2006. *J. Geophys. Res.* **113**, 1998–2006 (2008).
- Uitz, J., Claustre, H., Gentili, B. & Stramski, D. Phytoplankton class-specific primary production in the world's oceans: Seasonal and interannual variability from satellite observations. *Global Biogeochemical Cycles* **24**, GB3016 (2010).
- Arrigo, K. R. & van Dijken, G. L. Continued increases in Arctic Ocean primary production. *Prog. Oceanogr.* **136**, 60–70 (2015).
- Moore, C. M. *et al.* Processes and patterns of oceanic nutrient limitation. *Nat. Geosci.* **6**, 701–710 (2013).
- de Baar, H. J. W. *et al.* Importance of iron for plankton blooms and carbon dioxide drawdown in the Southern Ocean. *Nature* **373**, 412–415 (1995).
- Tremblay, J.-É & Gagnon, J. The effects of irradiance and nutrient supply on the productivity of Arctic waters: a perspective on climate change. In *Influence of Climate Change on the Changing Arctic and Sub-Arctic Conditions* (eds Nihoul, J. C. J. & Kostianoy, A. G.) 73–89 (Springer, Berlin, 2009).
- De Jong, J. T. M. *et al.* Sources and fluxes of dissolved iron in the Bellingshausen Sea (West Antarctica): the importance of sea ice, icebergs and the continental margin. *Mar. Chem.* **177**, 518–535 (2015).
- Popova, E. E. *et al.* What controls primary production in the Arctic Ocean? Results from an intercomparison of five general circulation models with biogeochemistry. *J. Geophys. Res. Ocean.* **117**, (2012).
- Nielsdóttir, M. C., Moore, C. M., Sanders, R., Hinz, D. J. & Achterberg, E. P. Iron limitation of the postbloom phytoplankton communities in the Iceland Basin. *Glob. Biogeochem. Cycles* **23**, 1–13 (2009).
- Ryan-Keogh, T. J. *et al.* Spatial and temporal development of phytoplankton iron stress in relation to bloom dynamics in the high-latitude North Atlantic Ocean. *Limnol. Oceanogr.* **58**, 533–545 (2013).
- Taylor, R. L. *et al.* Colimitation by light, nitrate, and iron in the Beaufort Sea in late summer. *J. Geophys. Res. Ocean.* **118**, 3260–3277 (2013).
- Findlay, H. S. *et al.* Late winter biogeochemical conditions under sea ice in the Canadian High Arctic. *Polar Res.* **34**, 24170 (2015).
- Mills, M. M. *et al.* Nitrogen limitation of the summer phytoplankton and heterotrophic prokaryote communities in the Chukchi Sea. *Front. Mar. Sci.* **5**, 1–22 (2018).
- Hopwood, M. J. *et al.* Non-linear response of summertime marine productivity to increased meltwater discharge around Greenland. *Nat. Commun.* **9**, 1–9 (2018).
- Codispoti, L. A. *et al.* Synthesis of primary production in the Arctic Ocean: III. Nitrate and phosphate based estimates of net community production. *Prog. Oceanogr.* **110**, 126–150 (2013).
- Schauer, U. *et al.* Variation of measured heat flow through the Fram Strait between 1997 and 2006. In *Arctic-Subarctic Ocean Fluxes: Defining the Role of the Northern Seas in Climate* (eds Dickson, R. R. *et al.*) 65–85 (Springer, Berlin, 2008).
- Mouginot, J. *et al.* Fast retreat of Zachariae Isstrøm, northeast Greenland. *Science* (80-,) **350**, 1357–1361 (2015).
- Smedsrud, L. H., Halvorsen, M. H., Stroeve, J. C., Zhang, R. & Kloster, K. Fram Strait sea ice export variability and September Arctic sea ice extent over the last 80 years. *Cryosphere* **11**, 65–79 (2017).
- Rijkenberg, M. J. A., Slagter, H. A., Rutgers Van Der Loeff, M., Ooijen, J. Van. & Gerringa, L. J. A. Dissolved Fe in the deep and upper Arctic Ocean with a focus on Fe limitation in the Nansen Basin. *Front. Mar. Sci.* **5**, 88 (2018).
- de Steur, L. *et al.* Freshwater fluxes in the East Greenland Current: a decade of observations. *Geophys. Res. Lett.* **36**, 1–5 (2009).
- Beszczyńska-Möller, A., Woodgate, R. A., Lee, C., Melling, H. & Karcher, M. A synthesis of exchanges through the main oceanic gateways to the Arctic Ocean. *Oceanography* **24**, 82–99 (2011).
- Rudels, B. Arctic ocean circulation. in *Encyclopedia of Ocean Sciences* 262–277 (Elsevier Inc., 2019). <https://doi.org/10.1016/B978-0-12-409548-9.11209-6>
- Laukert, G. *et al.* Ocean circulation and freshwater pathways in the Arctic Mediterranean based on a combined Nd isotope, REE and oxygen isotope section across Fram Strait. *Geochim. Cosmochim. Acta* **202**, 285–309 (2017).
- Michel, C. *et al.* Arctic Ocean outflow shelves in the changing Arctic: a review and perspectives. *Prog. Oceanogr.* **139**, 66–88 (2015).
- Rudels, B. *et al.* The interaction between waters from the Arctic Ocean and the Nordic Seas north of Fram Strait and along the East Greenland Current: Results from the Arctic Ocean-02 Ocean expedition. *J. Mar. Syst.* **55**, 1–30 (2005).
- Lalande, C. *et al.* Lateral supply and downward export of particulate matter from upper waters to the seafloor in the deep eastern Fram Strait. *Deep. Res. Part I Oceanogr. Res. Pap.* **114**, 78–89 (2016).

27. Norwegian Polar Institute. Sea ice extent in the Fram Strait in September, 1979–2018. *Environmental Monitoring of Svalbard and Jan Mayen (MOSJ)* (2020). <https://www.mosj.no/en/climate/ocean/sea-ice-extent-barents-sea-fram-strait.html>. Accessed 10th January 2020.
28. de Steur, L., Peralta-Ferriz, C. & Pavlova, O. Freshwater export in the East Greenland current freshens the North Atlantic. *Geophys. Res. Lett.* **45**, 13359–13366 (2018).
29. Marnela, M., Rudels, B., Houssais, M.-N., Beszczynska-Möller, A. & Eriksson, P. B. Recirculation in the Fram Strait and transports of water in and north of the Fram Strait derived from CTD data. *Ocean Sci.* **9**, 499–519 (2013).
30. Beszczynska-Möller, A., Fahrbach, E., Schauer, U. & Hansen, E. Variability in Atlantic water temperature and transport at the entrance to the Arctic Ocean, 1997–2010. *ICES J. Mar. Sci.* **69**, 852–863 (2012).
31. de Steur, L., Hansen, E., Mauritzen, C., Beszczynska-Möller, A. & Fahrbach, E. Impact of recirculation on the East Greenland Current in Fram Strait: Results from moored current meter measurements between 1997 and 2009. *Deep. Res. Part I Oceanogr. Res. Pap.* **92**, 26–40 (2014).
32. Grasshoff, K., Kremling, K. & Ehrhardt, M. *Methods of Seawater Analysis* (Wiley, Hoboken, 1999). <https://doi.org/10.1002/9783527613984>.
33. Cutter, G. *et al.* Sampling and Sample-handling Protocols for GEOTRACES Cruises. (2014).
34. Rapp, I., Schlosser, C., Rusiecka, D., Gledhill, M. & Achterberg, E. P. Automated preconcentration of Fe, Zn, Cu, Ni, Cd, Pb Co, and Mn in seawater with analysis using high-resolution sector field inductively-coupled plasma mass spectrometry. *Anal. Chim. Acta* **976**, 1–13 (2017).
35. Moore, C. M. Diagnosing oceanic nutrient deficiency. *Philos. Trans. R. Soc. A Math. Phys. Eng. Sci.* **374**, 20150290 (2016).
36. Browning, T. J. *et al.* Nutrient co-limitation at the boundary of an oceanic gyre. *Nature* **551**, 242–246 (2017).
37. Achterberg, E. P. *et al.* Natural iron fertilization by the Eyjafjallajökull volcanic eruption. *Geophys. Res. Lett.* **40**, 921–926 (2013).
38. Welschmeyer, N. A. Fluorometric analysis of chlorophyll a in the presence of chlorophyll b and pheopigments. *Limnol. Oceanogr.* **39**, 1985–1992 (1994).
39. Van Heukelem, L. & Thomas, C. S. Computer-assisted high-performance liquid chromatography method development with applications to the isolation and analysis of phytoplankton pigments. *J. Chromatogr. A* **910**, 31–49 (2001).
40. Mackey, M. D., Mackey, D. J., Higgins, H. W. & Wright, S. W. CHEMTAX - a program for estimating class abundances from chemical markers: application to HPLC measurements of phytoplankton. *Mar. Ecol. Prog. Ser.* **144**, 265–283 (1996).
41. Coupel, P. *et al.* Pigment signatures of phytoplankton communities in the Beaufort Sea. *Biogeosciences* **12**, 991–1006 (2015).
42. Hong, C. N. *et al.* Sediment efflux of silicon on the Greenland margin and implications for the marine silicon cycle. *Earth Planet. Sci. Lett.* **529**, 115877 (2020).
43. Tonnard, M. *et al.* Dissolved iron in the North Atlantic Ocean and Labrador Sea along the GEOVIDE section (GEOTRACES section GA01). *Biogeosciences* **17**, 917–943 (2020).
44. Colombo, M., Jackson, S. L., Cullen, J. T. & Orians, K. J. Dissolved iron and manganese in the Canadian Arctic Ocean: On the biogeochemical processes controlling their distributions. *Geochim. Cosmochim. Acta* (2020). (in press).
45. Ardiningsih, I. *et al.* Natural Fe-binding organic ligands in Fram Strait and over the Northeast Greenland shelf. *Mar. Chem.* **224**, (2020).
46. Le Moigne, F. A. C. *et al.* Sequestration efficiency in the iron-limited North Atlantic: implications for iron supply mode to fertilized blooms. *Geophys. Res. Lett.* **41**, 4619–4627 (2014).
47. Beszczynska-Möller, A. & Wisotzki, A. Physical oceanography during POLARSTERN cruise ARK-XXIII/2. *Alfred Wegener Institute, Helmholtz Centre for Polar and Marine Research, Bremerhaven, PANGAEA* (2010). <https://doi.org/10.1594/PANGAEA.733424>.
48. Kattner, G. & Ludwischowski, K.-U. Inorganic nutrients measured on water bottle samples during POLARSTERN cruise ARK-XXIII/2. *Alfred Wegener Institute, Helmholtz Centre for Polar and Marine Research, Bremerhaven, PANGAEA* (2014). <https://doi.org/10.1594/PANGAEA.832402>.
49. Randelhoff, A., Fer, I., Sundfjord, A., Tremblay, J. -É & Reigstad, M. Vertical fluxes of nitrate in the seasonal nitracline of the Atlantic sector of the Arctic Ocean. *J. Geophys. Res. Ocean.* **121**, 3010–3028 (2016).
50. Achterberg, E. P. *et al.* Iron biogeochemistry in the high latitude North Atlantic ocean. *Sci. Rep.* **8**, 1–15 (2018).
51. Torres-Valdés, S. *et al.* Export of nutrients from the Arctic Ocean. *J. Geophys. Res.* **118**, 1625–1644 (2013).
52. Ooijen, J. Van, Rijkenberg, M. J. A., Gerringa, L. J. A., Rabe, B. & van der Loeff, M. R. *Inorganic nutrients measured on water bottle samples during POLARSTERN cruise PS94 (ARK-XXIX/3)*. (2016). <https://doi.org/10.1594/PANGAEA.868396>
53. Slatger, H. A. *et al.* Organic Fe speciation in the Eurasian Basins of the Arctic Ocean and its relation to terrestrial DOM. *Mar. Chem.* **197**, 11–25 (2017).
54. Gerringa, L. J. A., Rijkenberg, M. J. A. & Slatger, H. A. *Dissolved iron measured on board with Flow injection analysis and iron-binding dissolved organic ligands from Ultra Clean CTD collected depth profiles during GEOTRACES PS94 Arctic cruise on Polarstern*. (2018). <https://doi.org/10.1594/PANGAEA.890975>
55. Krawczyk, D. W. *et al.* Seasonal succession, distribution, and diversity of planktonic protists in relation to hydrography of the Godthåbsfjord system (SW Greenland). *Polar Biol.* **41**, 2033–2052 (2018).
56. Meire, L. *et al.* High export of dissolved silica from the Greenland Ice Sheet. *Geophys. Res. Lett.* **43**, 9173–9182 (2016).
57. Nöthig, E.-M. *et al.* Summertime plankton ecology in Fram Strait: a compilation of long- and short-term observations. *Polar Res.* **34**, 1–18 (2015).
58. Moore, C. M. *et al.* Relative influence of nitrogen and phosphorus availability on phytoplankton physiology and productivity in the oligotrophic sub-tropical North Atlantic Ocean. *Limnol. Oceanogr.* **53**, 291–305 (2008).
59. Browning, T. J. *et al.* Nutrient co-limitation at the boundary of an oceanic gyre_Supplementary Material. *Nature* **551**, 242–246 (2017).
60. Kattner, G. & Budéus, G. Nutrient status of the Northeast Water Polynya. *J. Mar. Syst.* **10**, 185–197 (1997).
61. Smith, R. E. H., Gosselin, M. & Taguchi, S. The influence of major inorganic nutrients on the growth and physiology of high arctic ice algae. *J. Mar. Syst.* **11**, 63–70 (1997).
62. Maestrini, S. Y., Rochet, M., Legendre, L. & Demers, S. Nutrient limitation of the bottom-ice microalgal biomass (southeastern Hudson Bay, Canadian Arctic). *Limnol. Oceanogr.* **31**, 969–982 (1986).
63. Ortega-Retuerta, E., Jeffrey, W. H., Ghiglione, J. F. & Joux, F. Evidence of heterotrophic prokaryotic activity limitation by nitrogen in the Western Arctic Ocean during summer. *Polar Biol.* **35**, 785–794 (2012).
64. Mann, E. L. & Chisholm, S. W. Iron limits the cell division rate of *Prochlorococcus* in the eastern equatorial Pacific. *Limnol. Oceanogr.* **45**, 1067–1076 (2000).
65. Vernet, M. *et al.* Influence of phytoplankton advection on the productivity along the Atlantic water inflow to the Arctic Ocean. *Front. Mar. Sci.* **6**(583), 1–18 (2019).
66. Moore, C. M. *et al.* Iron limits primary productivity during spring bloom development in the central North Atlantic. *Glob. Chang. Biol.* **12**, 626–634 (2006).
67. Browning, T. J. *et al.* Nutrient regulation of late spring phytoplankton blooms in the midlatitude North Atlantic. *Limnol. Oceanogr.* **9999**, 1–13 (2019).
68. Blain, S. *et al.* Availability of iron and major nutrients for phytoplankton in the northeast Atlantic Ocean. *Limnol. Oceanogr.* **49**, 2095–2104 (2004).

69. Boyd, P. W. & Ellwood, M. J. The biogeochemical cycle of iron in the ocean. *Nat. Geosci.* **3**, 675–682 (2010).
70. Twining, B. S. & Baines, S. B. The trace metal composition of marine phytoplankton. *Ann. Rev. Mar. Sci.* **5**, 191–215 (2013).
71. Saito, M. A. *et al.* Multiple nutrient stresses at intersecting Pacific Ocean biomes detected by protein biomarkers. *Science* (80-) **345**, 1173–1177 (2014).
72. Ward, B. A., Dutkiewicz, S., Moore, C. M. & Follows, M. J. Iron, phosphorus, and nitrogen supply ratios define the biogeography of nitrogen fixation. *Limnol. Oceanogr.* **58**, 2059–2075 (2013).
73. Hattermann, T., Isachsen, P. E., Von Appen, W. J., Albretsen, J. & Sundfjord, A. Eddy-driven recirculation of Atlantic Water in Fram Strait. *Geophys. Res. Lett.* **43**, 3406–3414 (2016).
74. Klunder, M. B. *et al.* Dissolved iron in the Arctic shelf seas and surface waters of the central Arctic Ocean: impact of Arctic river water and ice-melt. *J. Geophys. Res. Ocean.* **117**, 1–18 (2012).
75. Charette, M. A. *et al.* The Transpolar Drift as a Source of Riverine and Shelf-Derived Trace Elements to the Central Arctic Ocean. *J. Geophys. Res. Ocean.* **125**, e2019JC015920 (2020).
76. Yamamoto-Kawai, M., Carmack, E. & McLaughlin, F. Nitrogen balance and Arctic throughflow. *Nature* **443**, 43 (2006).
77. Rijkenberg, M. J. A. *et al.* The distribution of dissolved iron in the West Atlantic Ocean. *PLoS ONE* **9**, 1–14 (2014).
78. de Boyer Montégut, C., Madec, G., Fischer, A. S., Lazar, A. & Iudicone, D. Mixed layer depth over the global ocean: an examination of profile data and a profile-based climatology. *J. Geophys. Res. Ocean.* **109**, 1–20 (2004).
79. Randelhoff, A., Sundfjord, A. & Reigstad, M. Seasonal variability and fluxes of nitrate in the surface waters over the Arctic shelf slope. *Geophys. Res. Lett.* **42**, 3442–3449 (2015).
80. Randelhoff, A. *et al.* Pan-Arctic ocean primary production constrained by turbulent nitrate fluxes. *Front. Mar. Sci.* **7**, 1–15 (2020).
81. Rafter, P. A., Sigman, D. M. & Mackey, K. R. M. Recycled iron fuels new production in the eastern equatorial Pacific Ocean. *Nat. Commun.* **8**, 1100 (2017).
82. Stohl, A. *et al.* Arctic smoke: record high air pollution levels in the European Arctic due to agricultural fires in Eastern Europe in spring 2006. *Atmos. Chem. Phys.* **7**, 511–534 (2007).
83. Marsay, C. M. *et al.* Concentrations, provenance and flux of aerosol trace elements during US GEOTRACES Western Arctic cruise GN01. *Chem. Geol.* **502**, 1–14 (2018).
84. Conca, E. *et al.* Source identification and temporal evolution of trace elements in PM10 collected near to Ny-Ålesund (Norwegian Arctic). *Atmos. Environ.* **203**, 153–165 (2019).
85. Kadko, D. *et al.* The residence times of trace elements determined in the surface Arctic Ocean during the 2015 US Arctic GEOTRACES expedition. *Mar. Chem.* **208**, 56–69 (2019).
86. Wehrmann, L. M. *et al.* Iron and manganese speciation and cycling in glacially influenced high-latitude fjord sediments (West Spitsbergen, Svalbard): evidence for a benthic recycling-transport mechanism. *Geochim. Cosmochim. Acta* **141**, 628–655 (2014).
87. Bown, J. *et al.* Evidences of strong sources of DFe and DMn in Ryder Bay, Western Antarctic Peninsula. *Philos. Trans. R. Soc. A Math. Phys. Eng. Sci.* **376**, 20170172 (2018).
88. Bucciarelli, E., Blain, S. & Tréguer, P. Iron and manganese in the wake of the Kerguelen Islands (Southern Ocean). *Mar. Chem.* **73**, 21–36 (2001).
89. Nishino, S. *et al.* Enhancement/Reduction of biological pump depends on ocean circulation in the sea-ice reduction regions of the Arctic Ocean. *J. Oceanogr.* **67**, 305–314 (2011).
90. Kipp, L. E., Charette, M. A., Moore, W. S., Henderson, P. B. & Rigor, I. G. Increased fluxes of shelf-derived materials to the central arctic ocean. *Sci. Adv.* **4**, 1–10 (2018).
91. Mayot, N. *et al.* Springtime export of Arctic Sea ice influences phytoplankton production in the Greenland Sea. *J. Geophys. Res. Ocean.* **125**, 1–16 (2020).
92. Randelhoff, A. *et al.* The evolution of light and vertical mixing across a phytoplankton ice-edge bloom. *Elem. Sci. Anthr.* **7**, 1–19 (2019).
93. Kahru, M., Brotas, V., Manzano-Sarabia, M. & Mitchell, B. G. Are phytoplankton blooms occurring earlier in the Arctic?. *Glob. Chang. Biol.* **17**, 1733–1739 (2011).
94. Ardyna, M. *et al.* Environmental drivers of under-ice phytoplankton bloom dynamics in the Arctic Ocean. *Elem. Sci. Anthr.* **8**, 30 (2020).
95. Tremblay, J. É. *et al.* Vertical stability and the annual dynamics of nutrients and chlorophyll fluorescence in the coastal, southeast Beaufort Sea. *J. Geophys. Res. Ocean.* **113**, 1–14 (2008).
96. Castro de la Guardia, L. *et al.* Assessing the role of high-frequency winds and sea ice loss on arctic phytoplankton blooms in an ice-ocean-biogeochemical model. *J. Geophys. Res. Biogeosci.* **124**, 2728–2750 (2019).
97. Ardyna, M. *et al.* Recent Arctic Ocean sea ice loss triggers novel fall phytoplankton blooms. *Geophys. Res. Lett.* **41**, 6207–6212 (2014).
98. Wang, Q. *et al.* Intensification of the Atlantic Water supply to the Arctic Ocean through Fram Strait induced by Arctic sea ice decline. *Geophys. Res. Lett.* **47**, e2019GL086682 (2020).
99. Arrigo, K. R., van Dijken, G. & Pabi, S. Impact of a shrinking Arctic ice cover on marine primary production. *Geophys. Res. Lett.* **35**, 1–6 (2008).
100. Carmack, E. C., Macdonald, R. W. & Steve, J. Phytoplankton productivity on the Canadian Shelf of the Beaufort Sea. *Mar. Ecol. Prog. Ser.* **277**, 37–50 (2004).
101. Lasternas, S. & Agustí, S. Phytoplankton community structure during the record Arctic ice-melting of summer 2007. *Polar Biol.* **33**, 1709–1717 (2010).
102. Harding, K. *et al.* Symbiotic unicellular cyanobacteria fix nitrogen in the Arctic Ocean. *Proc. Natl. Acad. Sci.* **115**, 13371–13375 (2018).
103. Sipler, R. E. *et al.* Preliminary estimates of the contribution of Arctic nitrogen fixation to the global nitrogen budget. *Limnol. Oceanogr.* **2**, 159–166 (2017).
104. Zehr, J. P. & Kudela, R. M. Nitrogen cycle of the open ocean: from genes to ecosystems. *Annu. Rev. Mar. Sci.* **3**, 197–225 (2011).
105. Acker, J. G. & Leptoukh, G. Online analysis enhances use of NASA Earth Science Data. *Eos (Washington, DC)* **88**, 14–17 (2007).
106. Schaffer, J. *et al.* A global, high-resolution data set of ice sheet topography, cavity geometry, and ocean bathymetry. *Earth Syst. Sci. Data* **8**, 543–557 (2016).

Acknowledgements

The authors thank Captain Schwarze and the crew of the RV Polarstern (GN05 cruise), operated by the Alfred Wegener Institute, Helmholtz Centre for Polar and Marine Research (AWI), Michiel Rutgers van der Loeff (AWI) and Nicola Herzberg (GEOMAR) for assistance with sample collection; Takamasa Tsubouchi (AWI), Janin Schaffer (AWI), Eike Köhn (GEOMAR) and Nat Wilson (Woods Hole Oceanographic Institution) for CTD handling; Gerd Rohardt (AWI) for CTD data processing; Kerstin Nachtigall (GEOMAR) for assistance with the HPLC measurements; Christian Schlosser and Shao-Min Chen (GEOMAR) for assistance during micronutrient analyses. S.K. was financed by GEOMAR and the German Research Foundation (DFG Award Number

AC 217/1-1 to E.P.A). T.J.B. acknowledges funding from a Marie Skłodowska-Curie Postdoctoral European Fellowship (OceanLiNES; Project ID 658035).

Author contributions

S.K., T.J.B. and E.P.A. designed the research. Sampling and analyses were performed by S.K., M.G., K.U.L., P.L., S.R., J.C.Y. and T.K. The manuscript was written by S.K. and T.J.B. with all authors contributing to its revision.

Funding

Open Access funding provided by Projekt DEAL.

Competing interests

The authors declare no competing interests.

Additional information

Supplementary information is available for this paper at <https://doi.org/10.1038/s41598-020-72100-9>.

Correspondence and requests for materials should be addressed to E.P.A.

Reprints and permissions information is available at www.nature.com/reprints.

Publisher's note Springer Nature remains neutral with regard to jurisdictional claims in published maps and institutional affiliations.



Open Access This article is licensed under a Creative Commons Attribution 4.0 International License, which permits use, sharing, adaptation, distribution and reproduction in any medium or format, as long as you give appropriate credit to the original author(s) and the source, provide a link to the Creative Commons licence, and indicate if changes were made. The images or other third party material in this article are included in the article's Creative Commons licence, unless indicated otherwise in a credit line to the material. If material is not included in the article's Creative Commons licence and your intended use is not permitted by statutory regulation or exceeds the permitted use, you will need to obtain permission directly from the copyright holder. To view a copy of this licence, visit <http://creativecommons.org/licenses/by/4.0/>.

© The Author(s) 2020